Liquid DNA coacervates form porous capsular hydrogels via viscoelastic phase separation on microdroplet interface

Masamune Morita,[†a] *Tetsuro Sakamoto,*[a] *Shin-ichiro M. Nomura,*[b] *Satoshi Murata,*[b] *Miho Yanagisawa,**[c] *and Masahiro Takinoue**[a,d,e]

[a] Department of Computer Science, Tokyo Institute of Technology, 4259 Nagatsuta-cho, Midori-ku, Yokohama 226-8501, Japan

[b] Department of Bioengineering and Robotics, Tohoku University, 6-6-01 Aoba-yama, Sendai 980-8579, Japan

[c] Komaba Institute for Science, Graduate School of Arts and Sciences, The University of Tokyo, 3-8-1 Komaba, Meguro, Tokyo 153-8902, Japan

[d] Department of Life Science and Technology, Tokyo Institute of Technology, 4259 Nagatsuta-cho, Midori-ku, Yokohama 226-8501, Japan

[e] Living Systems Materialogy (LiSM) Research Group, International Research Frontiers Initiative (IRFI), Tokyo Institute of Technology, 4259, Nagatsuta-cho, Midori-ku, Yokohama 226-8501, Japan

KEYWORDS: DNA liquid, DNA droplet, viscoelastic phase separation, water-in-oil microdroplet, microdroplet interface

ABSTRACT

Liquid-liquid phase separation (LLPS) droplets of biopolymers are known as functional microdroplets in living cells and have recently been used to construct protocells and artificial cells. The formation of DNA coacervates (also referred to as DNA droplets) from branched DNA nanostructures and the control of their physical properties via DNA nanostructure design were demonstrated previously. For the construction of artificial cells or protocells, however, even though physical effects such as surface tension, wetting, and viscoelasticity are more important in a tiny (micrometer-sized), confined environment than in a bulk solution environment, they have not been explored yet. This study shows that a tiny, confined environment using a water-in-oil (W/O) microdroplet interface modulates the phase separation dynamics of DNA coacervates, leading to micrometer-sized porous capsular structures. The porous structures were produced via two types of viscoelastic phase separation (VPS) processes in DNA coacervates: (i) simple VPS and (ii) cluster-cluster aggregation after VPS. Finally, it was shown that environmental chemical stimulation can manipulate porous capsular DNA hydrogels extracted from W/O microdroplets. These results provide an approach for designing and fabricating artificial cells or protocells with complex structures and physicochemical properties.

INTRODUCTION

Liquid-liquid phase separation (LLPS) droplets of biopolymers have been studied for a long time in terms of the origins of life[1,2], protocell models[3–8], and in artificial cell engineering[9–11]. The LLPS droplets in living cell[12,13] such as nucleoli, P-bodies, and stress granules, are membrane-less organelles that exert a variety of biological functions[14] such as sensing, localization, and concentration of molecules, and activation or inactivation of biomolecular reactions. One of the LLPS droplets is an aqueous two-phase system droplet formed via the segregation of aqueous polymers, such as polyethylene glycol (PEG) and dextran[2,15–21], which is also referred to as a non-associative LLPS droplet. Another LLPS droplet is a coacervate (also called an associative LLPS droplet), which is formed via associative interactions between biopolymers. For example, intrinsically disordered regions of proteins[22], nucleic acid base pairings[23–26], and charged biopolymers[3–6,27–29] have been reported as dominant factors for associative interactions.

The typical structure of biopolymer coacervates are spherical droplets; however, they can have porous structures that occur via interactions with other intracellular structures, such as the nuclear membrane. For example, the viscoelastic phase separation (VPS)[30–33] of chromatins partly tethered to the cell nuclear membrane is expected to be used to form a sponge-like chromatin structure[34]. Like this, the interaction between biopolymer coacervates and a tiny, confined environment often plays essential roles in self-organized structure formations.

Recently, DNA nanotechnology[35] has demonstrated the formation of liquid-like DNA coacervates[24–26,28,29,36–48] (DNA droplets), which have attracted interest as design-based

methods for forming and controlling biopolymer coacervates. DNA nanotechnology relies on the programmability of DNA sequences based on the computational prediction of the thermodynamic stability of base pairing and the physical topology of DNA strings[49–51] and has achieved DNA nanostructures[35,52], DNA hydrogels[53–56], and assemblies of DNA nanostructures on lipid membranes or oil-water interfaces[57–61]. The established knowledge of DNA nanotechnology has been applied to the design and formation of DNA droplets[47] constructed with branched DNA nanostructures (called DNA motifs or DNA nanostars)[23–26, 36–41, 43–46], and multi-block long single-stranded DNA (ssDNA) generated by rolling-circle amplification[62–64]. These studies also demonstrated the dynamic behavior of DNA droplets[48], such as phase separation and the division of two immiscible DNA droplets with orthogonal sequences[36,37], bubbling of DNA droplets with an enzymatic reaction[38], disruption of lipid membranes[39], DNA logic computation[40], and droplet locomotion[45,64].

In addition, the dynamics of DNA coacervates can be altered by interactions with surfaces or tiny, confined spaces. For example, Sato et al. demonstrated that immiscible DNA coacervates exhibited an ordered lateral pattern formation by interacting with a liposome inner surface[65], even though the immiscible DNA coacervates showed a simple division in an uncontrolled manner in a bulk solution. Tran et al. demonstrated that a DNA droplet was divided into two droplets in a controlled manner if it was encapsulated in a tiny, confined space with liposome[66]. Leathers et al. demonstrated a reaction-diffusion pattern in a small DNA droplet[41]. However, modulation of the dynamics of DNA coacervates remains challenging because it enables the construction of artificial cells or protocells with more complex structures and functions.

Herein, we report that modulating the dynamics of DNA coacervates on the lipid monolayer interface of water-in-oil (W/O) microdroplets leads to porous pattern formation. The DNA coacervates are formed by the self-assembly of Y-shaped branched DNA nanostructures (DNA Y-motifs) on the W/O microdroplet interface by annealing. This process generates micrometer-sized capsular structures of the DNA coacervate. Porous or non-porous DNA coacervates were formed depending on the DNA Y-motif concentration and the cooling rate of annealing. The experiments revealed that a porous structure was produced by the phase separation of DNA coacervates based on the VPS. Finally, applying the phase-separated porous structures showed that the porous capsular DNA hydrogels can be dynamically manipulated after their extraction from W/O microdroplets.

RESULTS AND DISCUSSION

Formation of porous/non-porous structures of capsular DNA coacervates on a lipid monolayer interface of a W/O microdroplet

Figure 1A shows a schematic representation of the formation of liquid- and gel-like DNA coacervates with three single-stranded DNAs (ssDNA1, ssDNA2, and ssDNA3)[36,46,61,65]. The ssDNAs were completely dissociated when the solution temperature $T > T_{mY}$ (T_{mY}: melting temperature of the Y-motif stem). Dispersed DNA Y-motifs are formed when $T_{mY} > T > T_L$ (T_L: formation temperature of liquid-like DNA coacervates). Liquid-like DNA coacervates are formed when $T_L > T > T_G$ (T_G: formation temperature of gel-like DNA coacervates), where the Y-motifs bind to one another via the dynamic repetition of attachment and detachment of their sticky ends. When $T_G > T$, gel-like DNA coacervates were formed by static binding of the Y-motifs via their sticky ends (Figure 1A, right). DNA sequences were designed using the

Nucleic Acid Package (NUPACK)[49]. Numerically calculated T_{mY} and T_{mS} (melting temperature of sticky ends) are ~75°C and ~46°C, respectively, and the measured T_L and T_G were ~64°C and ~35°C, respectively[36], in our experimental condition for DNA coacervate formation (several μM ssDNAs, 20 mM Tris-HCl buffer (pH 8.0), 350 mM NaCl).

In this study, we encapsulated a DNA Y-motif solution in a W/O microdroplet. We investigated the pattern-formation dynamics that emerged from the interaction between DNA coacervates and the lipid monolayer interface of the W/O microdroplet (Figure 1B). The lipid monolayer interface is composed of two types of lipids: a zwitterionic lipid, 1,2-dioleoyl-sn-glycero-3-phosphocholine (DOPC) and a cationic lipid, 1-oleoyl-2-{6-[(7-nitro-2-1,3-benzoxadiazol-4-yl)amino]hexanoyl}-sn-glycero-3-phosphocholine (DOTAP). The total lipid concentration was 2 mM. By the annealing of the emulsion of W/O microdroplets from 95°C ($> T_{mY}$) to 20°C ($< T_G$), the DNA coacervates formed by self-assembly from the DNA Y-motifs on the microdroplet interface via electrostatic interaction between the anionic DNA molecules and the cationic interfacial lipids results in the formation of porous/non-porous structures of capsular DNA coacervates[65]. It has been reported that the wettability of polymers to a microdroplet interface affects the pattern-formation of a polymer gel at the microdroplet interface[66–68]. In this study, we investigated the dependence of the pattern-formation of capsular DNA coacervates on the wettability of the DNA coacervates to the interface by changing the ratio of DOTAP composition in total lipid from 100% to 50% (Figure S1). When DOPC:DOTAP = 0:100, only non-porous structures of capsular DNA coacervates were observed because the wettability of the DNA coacervates to the interface was strong. As the ratio of the DOTAP decreased, the percentage of porous structures of the capsular DNA coacervates increased due

to the wettability of the DNA coacervate to the interface became weaker. Hereafter, the lipid composition in the oil phase was fixed to DOPC:DOTAP = 50:50 in all experiments.

Figure 2 shows three-dimensionally (3D) reconstructed images of the capsular DNA coacervates formed on the microdroplet interface. The images were obtained using a confocal laser scanning microscope (CLSM) at various DNA concentrations and cooling rates. As shown in Figures 2A–D, each concentration of ssDNA1, ssDNA2, and ssDNA3 was C_{DNA}= 10 μM. It was found that round porous (Figures 2A and 2B) and non-porous (Figures 2C and 2D) capsular DNA coacervates were formed at each cooling rate, r_c= 0.01 and 0.5°C s^{-1}, respectively. Figure 2E summarizes the formation percentages of porous/non-porous structures of capsular DNA coacervates depending on the cooling rate r_c. When $r_c \leq$ 0.05°C s^{-1}, the round-porous structures were more frequent than non-porous structures. In contrast, the non-porous structures were formed more frequently when $r_c \geq$ 0.1°C s^{-1}. Capsular DNA coacervates tended to be more homogeneous (i.e., non-porous) at faster cooling rates.

Next, the dependence of the structures of capsular DNA coacervates on different DNA concentrations was investigated. Figures 2F–2I show the formation results of capsular DNA coacervates in a lower DNA concentration (C_{DNA}= 5 μM for each ssDNA1-3). As a result of CLSM observations, jagged porous (Figures 2F–2G) and non-porous (Figures 2H–2I) capsular DNA coacervates were found at a cooling rate r_c= 0.01 and 0.1°C s^{-1}, respectively. Interestingly, the pore shape was not circular, unlike in the presence of 10 μM DNA. Figure 2J summarizes the percentage of each structure of the capsular DNA coacervates depending on r_c. Similar to the conditions of 10 μM DNA, more homogeneous structures were formed at the faster cooling, though the pore shapes were different.

Generally, DNA annealing processes produce a homogeneous DNA structure because it is thermodynamically the most stable structure. Thus, it was expected that a slower cooling rate (annealing rate) would make DNA coacervates non-porous (i.e., homogeneous), and a faster cooling rate would make them porous, but the obtained results showed the opposite. Therefore, it was speculated that the porous structure was not formed via thermodynamic equilibrium; the kinetic processes of DNA coacervation/gelation under non-equilibrium conditions or the interactions with the microdroplet interface must have affected the porous/non-porous structure formations.

Investigation of the formation mechanism of porous/non-porous structures of capsular DNA coacervates

To investigate whether the microphase separation of lipids affected the formation of porous structures of capsular DNA coacervates, we first observed the distribution of cationic lipids (DOTAP) at the oil-water interface of the microdroplet. Figure 3A shows a comparison between the positions of DNA and DOTAP, where DNA was stained with 4',6-diamidino-2-phenylindole (DAPI; blue) and the cationic lipid was stained with a fluorescent variant of DOTAP, 1-oleoyl-2-[6-[(7-nitro-2-1,3-benzoxadiazol-4-yl)amino]hexanoyl]-3-trimethylammonium propane (NBD-DOTAP; green). These results demonstrated that the cationic lipids were distributed homogeneously, even though the DNA had a porous structure. It was not that the lipid monolayer interface formed the inhomogeneity of the DNA coacervate.

Next, a real-time observation of the formation process of the capsular DNA coacervates during decreasing temperatures from 80°C to 30°C was performed (Figure 3B). Figure 3B shows the fluorescently observed DNA Y-motif distribution (white areas in grayscale images) on the microdroplet interface. The dispersed DNA Y-motifs first accumulated homogeneously on the microdroplet interface by the electrostatic interaction between DNA and cationic lipids, even at a temperature higher than T_L (~64°C). The accumulated DNA Y-motifs connected at temperatures lower than T_L, resulting in liquid-like DNA coacervates. Figures 3B-(i) shows the results in the conditions that the round porous structures of capsular DNA coacervates tended to be formed (C_{DNA}= 10 μM, slower cooling rate: r_c = 0.01°C s^{-1}). It was found that microphase separation of the DNA coacervate at the microdroplet interface was involved in the formation of DNA coacervates (Figure 3B-(i)). Many micrometer-sized pores were formed by microphase separation as the temperature decreased; subsequently, the micropores expanded or fused (Figure 3B-(i)). These pore structures correspond to the round porous structures shown in Figures 2A, 2B, and 3A-(i). In contrast, at a faster cooling rate (r_c = 0.33°C s^{-1}), the DNA distribution on the microdroplet interface was kept homogeneous (Figure 3B-(ii)).

Real-time observations of the pore formation process at a lower DNA concentration were also performed, where the jagged porous structures of capsular DNA coacervates tended to form (C_{DNA}= 5 μM, slower cooling rate: r_c = 0.01°C s^{-1}). It was found that small DNA coacervate particles were formed by microphase separation at the microdroplet interface; the coacervate particles and their clusters then diffused and aggregated to form heterogeneous structures at the microdroplet interface (Figure 3B-(iii)). These heterogeneous structures correspond to the jagged porous structures shown in Figures 2F, 2G, and 3A-(ii). In contrast, when the non-porous structures of capsular DNA coacervates were formed (C_{DNA}= 5 μM, faster cooling rate:

r_c = 0.1°C s^{-1}), the DNA distribution on the microdroplet interface remained homogeneous (Figure 3B-(iv)).

Fractal analysis was performed on the jagged porous structures of the capsular DNA coacervates (Figure 3C). The fractal-dimension values were calculated using the box-counting method. The 3D microscopic images of the capsular DNA coacervates were first binarized, then their reconstructed images on a spherical surface were obtained (Figure 3C-(i)). Next, the box-counting method gave the fractal dimension on a spherical surface (Figure 3C-(ii)). The plotted points were on a linear line, suggesting that the capsular DNA coacervates have a fractal-like structure with a fractal dimension value of 1.7 (less than 2-dimensional). The observed aggregation of the coacervate particles and clusters (Figure 3B-(iii)) and the fractal analysis (Figure 3C-(ii)) suggest that the jagged porous structures of capsular DNA coacervates were formed by cluster-cluster aggregation (Supplementary Note 1 shows the numerical simulation of a cluster-cluster aggregation on a spherical surface).

In summary, these results revealed that there were two types of porous formations driven by different microphase separation processes depending on the DNA concentrations: (i) simple phase separation and (ii) cluster-cluster aggregation after phase separation (Figure 4). In general, soft matter systems exhibit transient porous structures of minor slower-diffusion components in major faster-diffusion components through the VPS[30–33], which include two typical processes depending on the concentration of the slower-diffusion components[33]. The phase separation results from this study were also considered VPS because the DNA Y-motif and solvent molecules would correspond to slower and faster diffusion components, respectively. At higher DNA concentrations (C_{DNA}= 10 μM), the DNA Y-motifs formed a

transient continuous liquid-like coacervate while expelling the solvent molecules. Then, the DNA coacervate phase-separates in a viscoelastic manner to form many round porous structures (Figure 4), similar to the sponge-like porous structure of general soft matter[33]. In contrast, at a lower DNA concentration (C_{DNA}= 5 μM), DNA Y-motifs formed transient discrete coacervate particles by VPS; the discrete DNA coacervate particles showed cluster-cluster aggregation to form jagged porous structures (Figure 4), similar to the network-like porous structure of general soft matter[33].

Analysis of the effect of the microdroplet interface on the VPS of DNA coacervates

The formation process of the porous structures of capsular DNA coacervates was different from that of typical DNA hydrogel microparticles because the DNA hydrogel microparticles were formed anywhere in the bulk solution by nucleation and growth if there was no microdroplet interface (Figure 1A). Therefore, the accumulation of DNA Y-motifs at the microdroplet interface of W/O microdroplets changed the gel formation process of DNA Y-motifs from nucleation and growth to VPS with the two types of microphase separation. To investigate the effect of the microdroplet interface, we further analyzed the VPS process of the DNA coacervates.

The dependence of the formation percentages of the round porous structures (C_{DNA}= 10 μM) on the W/O microdroplet radius (R) was investigated since the surface-to-volume ratio of the microdroplets ($4\pi R^2 / \left(\frac{4}{3}\pi R^3\right) \propto R^{-1}$) critically affects the physical properties of soft matter on the microdroplet surface in a nano/micrometer scale. Figure 5A shows 100% stacked bar charts of porous/non-porous structures of capsular DNA coacervates depending on the radius

of W/O microdroplets at each cooling rate (r_c = 0.01, 0.05, 0.1, and 0.5°C s^{-1}). As the radius of the W/O microdroplets increased, the percentage of round porous structures of the capsular DNA coacervates increased, regardless of the cooling rate.

Figure 5B shows a possible model explaining the Figure 5A results in terms of the relationship between the W/O microdroplet radius and the wettability of the DNA coacervate to the W/O microdroplet interface. If the wettability of DNA coacervate to the interface increases, the DNA coacervates prefer to spread on the interface; thus, the wettability would act as friction against the DNA coacervate phase separation. However, because the wettability affects only the surface of the DNA coacervate attached on the lipid monolayer, the DNA coacervate far from the microdroplet interface does not feel the friction so strongly; thus, the apparent friction against the DNA phase separation decreases with the DNA coacervate thickness (d) (Figure 5B). Here, we consider the dependence of d on the W/O microdroplet radius (R). C_{initial} and $C_{\text{coacervate}}$ denote the initial concentration of the DNA Y-motif in W/O microdroplets before coacervation and the DNA Y-motif concentration of the DNA coacervate on the microdroplet interface, respectively ($C_{\text{initial}} < C_{\text{coacervate}}$). Assuming that all DNA Y-motifs accumulate on the microdroplet interface and that $C_{\text{coacervate}}$ does not depend on the W/O microdroplet radius, the conservation of the total amount of DNA Y-motifs before and after coacervation gives

$$\frac{4}{3}\pi R^3 C_{\text{initial}} = \left(\frac{4}{3}\pi R^3 - \frac{4}{3}\pi(R-d)^3\right) C_{\text{coacervate}}.$$

We have

$$d = R\left(1 - \sqrt[3]{1 - \frac{C_{\text{initial}}}{C_{\text{coacervate}}}}\right),$$

which indicates d increases proportionally to R. This means the friction decreases with the microdroplet radius (R) increased (Figure 5B). Therefore, the VPS process would be

accelerated in the larger W/O microdroplets, resulting in the increase in the percentage of porous structures in the larger W/O microdroplets (Figure 5B). This hypothesis is also supported by Figure S1, which indicates the lower DOTAP ratio condition (i.e., less electrostatic interaction, less wettability, and less friction) resulted in a higher probability of porous structure formation.

This hypothesis was evaluated using a numerical model. To numerically analyze the formation process of round porous structures of capsular DNA coacervates, we extended Araki and Tanaka's disconnectable spring model[32] for the VPS of soft matter (Supplementary Note 2). The disconnectable spring model is a type of Brownian dynamics simulation model based on the overdamped Langevin equation for coarse-grained particles representing representative points of soft matter.

$$\zeta \frac{d}{dt}\boldsymbol{x}_i = -\boldsymbol{\nabla}_i U_{\mathrm{tot}}(\boldsymbol{x}_i) + \boldsymbol{\xi}_i \,, \tag{1}$$

where $\boldsymbol{x}_i$ is a normalized position of i-th coarse-grained particle in a DNA coacervate; t is the normalized simulation time; ζ is a normalized friction constant; $\boldsymbol{\xi}_i$ is a normalized thermal noise force ($\langle \boldsymbol{\xi}_i \rangle = 0$ and $\langle \boldsymbol{\xi}_i(t)\boldsymbol{\xi}_j(t') \rangle = 2T\zeta\delta_{ij}\delta(t-t')\boldsymbol{I}$; $\boldsymbol{I}$ is the identity matrix); T is the normalized 'virtual' temperature of the system; U_{tot} is a total potential composed of (i) the sum of the Lennard-Jones (LJ) potential between all pairs of particles and (ii) the sum of the harmonic potential representing elastic energy between particles connected with a spring. Here, the friction against DNA coacervate phase separation is assumed to decrease with the microdroplet radius as the above hypothesis. The connected particles can be stochastically disconnected with a disconnection rate $p(l_{ii'}) = \Delta t^{-1} e^{-\Delta E(l_{ii'})/T}$, where $\Delta E(l_{ii'}) = E_0 - \frac{1}{2}\kappa {l_{ii'}}^2$; $l_{ii'}$ is the extension length of the spring between i-th and i'-th particles; Δt is the time

step of simulation; E_0 decides the intrinsic disconnection rate without spring extension at the normalized temperature T: $p(0) = \Delta t^{-1} e^{-E_0/T}$. That is, the disconnection probability depends on the ratio of the stored elastic energy $\frac{1}{2}\kappa {l_{ii'}}^2$ to thermal energy ($\propto T$)[32]. Once the particles are disconnected, they remain unconnected. In contrast to the original model, the temperature was not constant when analyzing the annealing process of DNA coacervates in this study. Thus, the model was extended under the assumption that the temperature linearly decreased as follows:

$$T = T_0(1 - k_c t)\,, \qquad (2)$$

where T_0 is the initial normalized temperature and k_c is the cooling rate in numerical simulation; the calculation was performed during $0 \leq t \leq k_c^{-1}$. In addition, the motion of the particles was constrained to a spherical surface to mimic the W/O microdroplet interface (Supplementary Note 2). Equation (1) was solved using the Euler-Maruyama method as follows:

Numerical simulation of the structure of DNA coacervates has been performed by changing two parameters, the cooling rate k_c and the friction constant ζ. Figure 5C shows the numerically simulated structure of the DNA coacervate. The friction constant (horizontal axis) decreased from left to right, corresponding to an increase in the W/O microdroplet size. The simulation results show that the DNA coacervates tend to be more porous in the case of a smaller frictional force, which suggests that more porous DNA coacervates are obtained in the case of larger microdroplets, as shown in Figure 5A. When the cooling rate k_c (vertical axis) decreases from bottom to top, as shown in Figure 5C, the DNA coacervates tend to be more porous because there is sufficient disconnection between particles that causes the VPS before gelation at a low temperature. These results support the bar chart data for the DNA coacervate structures (Figure 5A). Thus, the hypothesis of this study would be reasonable.

Extraction and manipulation of capsular DNA coacervates in an aqueous solution

To produce DNA microcapsules, gelated capsular DNA coacervates were extracted from the W/O microdroplets by removing the oil phase and placing them in an aqueous buffer solution. Figures 6A and 6B show the extracted round porous and non-porous DNA microcapsules, respectively (see Supplementary Movies 5 and 6). It was confirmed that the extracted DNA microcapsules were not coated with lipids (Figure S2). Therefore, the DNA microcapsules were self-standing in the aqueous solution.

Next, to investigate the chemical–mechanical responsivity of the round porous DNA microcapsules, PEG (final concentration of ~1.25%) was added to a surrounding buffer solution of the round porous DNA microcapsules. Figure 6C shows the time-lapse images of the 3D-reconstructed CLSM images of the shrinkage of the round porous DNA microcapsules after the addition of PEG. Interestingly, during shrinkage, the shapes of the round porous DNA microcapsules were similar. In contrast, although the same experiments were done for regular DNA hydrogel microparticles, they hardly shrank even after adding the PEG solution (Figure 6D). The size of the round porous DNA microcapsules 15 min after the addition of PEG decreased to ~34% in diameter (~4% in volume) (Figure 6E), and the size of the microparticles decreased to ~94% in diameter (~83% in volume). This shrinkage was probably induced by the osmotic pressure exerted inside and outside the DNA hydrogels. After the removal of PEG from the solution, the round porous DNA microcapsules did not recover. These results suggest that the round porous DNA microcapsule was soft and that the mesh structures of the DNA hydrogel may have been rearranged. This result demonstrated that the round porous DNA

microcapsules had chemical–mechanical responsivity and their size could be tuned depending on the chemical environment.

CONCLUSIONS

From the results of this study, it can be shown that a DNA coacervate composed of DNA Y-motif nanostructures formed porous and non-porous microstructures through phase separation at the lipid monolayer interface of a W/O microdroplet (Figures 2 and 4). Microscopic observations (Figure 3) revealed that the cooling rate led to the formation of a porous or non-porous structure of capsular DNA coacervates. This is because competition between the VPS and gelation speeds of the DNA coacervate determines the nonequilibrium structure during the phase separation process.

Moreover, it was found that the formation of either the jagged or the round porous structures depended on the DNA Y-motif concentration (Figures 2 and 3). Soft matter systems generally exhibit two typical VPS processes depending on the concentration of minor slower-diffusion components such as DNA Y-motifs. First, the minor slower-diffusion components with lower concentrations form transient droplet-like discrete coacervates by phase separation while expelling the major faster-diffusion components such as water. Then, the discrete coacervates show Brownian diffusion and aggregate with one another to form a network-like porous structure[33] such as the jagged porous structures. On the other hand, the minor slower-diffusion components with higher concentrations formed a transient liquid-like continuous coacervate by phase separation while expelling the major component, and the continuous coacervate further phase-separated in a viscoelastic manner to form a sponge-like porous structure[33] such

as the round porous structures. The numerical simulation results (Figure 5C) supported the experimental results and this general feature of the VPS.

The DNA VPS coacervates on the microdroplet interface were key in forming complex hierarchical structures, such as porous DNA microcapsules. In this study, the diffusion of the DNA Y-motif was considered to be limited by the microdroplet interface friction, and the difference in the diffusion rate between the DNA Y-motif and surrounding small molecules was enhanced, resulting in the formation of the VPS pattern, which was not observed in bulk solution experiments before[36]. In addition, the dependence of the porous pattern formation on the microdroplet radius can be interpreted in terms of the wettability of the DNA coacervate to the microdroplet interface; i.e., the decrease in the wettability of the DNA coacervate to the surface with the increase of the microdroplet radius would result in the preferable formation of porous structures of capsular DNA coacervates.

Finally, it was shown that the porous or non-porous structures of the capsular DNA coacervates can be extracted into an aqueous solution and maintain their shape (Figure 6). These results offer an approach for designing and fabricating artificial cells or protocells with more complex structures and functions based on the VPS processes of DNA coacervates. In addition, Figure 6C shows that the extracted DNA microcapsules shrank while maintaining their shape similarity under osmotic pressure. This stimulus responsivity enables the development of molecular-responsive systems with DNA aptamers[69] and molecular-mechanical systems with DNA actuators[70]. In addition, DNA molecular devices capable of molecular computing using DNA logic gates[40,71,72] can be implemented in our DNA microcapsules. This study is believed to provide a new approach for developing dynamic capsule structures for artificial cells[61] and molecular robotics[73].

EXPERIMENTAL SECTION

Materials

Three designed ssDNA sequences (ssDNA1: GCTCGAGCCAGTGAGGACGGAAGTTTGTCGTAGCATCGCACC; ssDNA2: GCTCGAGCCAACCACGCCTGTCCATTACTTCCGTCCTCACTG; ssDNA3: GCTCGAGCGGTGCGATGCTACGACTTTGGACAGGCGTGGTTG) were purchased from Eurofins Genomics (Tokyo, Japan). DOPC (850375P), DOTAP (890890P), and NBD-DOTAP (810890P) were purchased from Avanti Polar Lipids, Inc. (Alabaster, Al, USA) as powder stocks. Mineral oil (23334-85) was purchased from Nacalai Tesque, Inc. (Kyoto, Japan). Tris-HCl buffer (pH 8.0) was purchased from Invitrogen (Carlsbad, CA, USA). Chloroform, methanol, sodium chloride (NaCl), and polyethylene glycol (PEG; Mw=300,000–500,000) were purchased from Wako Pure Chemical, Inc. (Osaka, Japan). Deionized (DI) water was obtained using a Millipore Milli-Q system.

Formation of DNA hydrogel microparticles in bulk solutions

Twenty microliters of DNA solution containing 5 μM of the three ssDNAs, 20 mM Tris-HCl buffer (pH 8.0), 350 mM NaCl, and 1× SYBR® Gold were prepared in a PCR tube. DNA microparticles were synthesized using a thermal cycler (T Gradient, Biometra, Göttingen, Germany). For the preparation of the DNA hydrogel microparticles, the DNA solution was annealed by reducing the temperature from 95°C to 20°C at the cooling rate r_c= 0.01°C s^{-1}

Preparation of an oil phase containing lipids

Forty microliters of lipid mixture of DOPC and DOTAP (10 mM each) in a chloroform:methanol solvent (2:1, in volume ratio) were poured into a glass tube. The lipid composition of DOPC and DOTAP (DOPC:DOTAP) was DOPC:DOTAP = 0:100, 10:90, 20:80, 30:70, 40:60, and 50:50, respectively. The organic solvent was evaporated by airflow to form a dry film at the bottom of the glass tube. The tube was then placed in a desiccator for 60 min. Mineral oil (200 μL) was added to the glass tube. Finally, the glass tube was sonicated in an ultrasonicator (ASU-3, AS ONE, Osaka, Japan) at 40°C for 60 min. The final lipid concentration was 2 mM.

Formation of the capsular DNA coacervates on the interface of the W/O microdroplet

Twenty microliters of DNA solution containing 5 or 10 μM of the three ssDNAs, 20 mM Tris-HCl buffer (pH 8.0), 350 mM NaCl, 1× SYBR® Gold was prepared. Two microliters of the DNA solution were added to the lipid-containing oil (50 μL) in a PCR tube, and the mixture was emulsified manually to obtain W/O microdroplets. Capsular DNA coacervates were formed using a thermal cycler. The DNA solution inside the W/O microdroplets was annealed by reducing the temperature from 95°C to 20°C at each cooling rate.

Imaging of the capsular DNA coacervates on the interface of the W/O microdroplet

Fluorescence imaging of the DNA microstructure was performed using a confocal laser scanning microscope (IX81, FV-1000; Olympus, Tokyo, Japan) with a UPLSAPO 40× objective lens. A DNA-specific fluorescent dye (SYBR® Gold or DAPI) was used to stain the

DNA microstructures. Five microliters of the W/O microdroplet solution were poured on silicon-coated glass (30×40×0.17 mm, Matsunami Glass Ind., Osaka, Japan). Confocal images were recorded, and Z stacks were collected and analyzed using software (FV-10-ASW 1.7, Olympus, Tokyo, Japan).

Real-time observation of the formation process of the capsular DNA coacervates on the microdroplet interface

Formation of capsular DNA coacervates was observed using a fluorescence microscope (IX71, Olympus, Tokyo, Japan) with a LUCPLFLN 20× objective lens. A DNA-specific fluorescent dye (SYBR® Gold) was used to stain DNA microstructures. Fluorescence images were recorded using a scientific complementary metal oxide semiconductor (sCMOS) camera (Zyla 4.2 plus; Andor, Belfast, UK). The sample temperature was controlled with a computer using a Peltier cooling/heating stage with a thermocouple (10021; Linkam Scientific Inst., Tadworth, UK).

Extraction of the capsular DNA coacervates from W/O microdroplets to an aqueous solution

Twenty microliters of DNA solution containing 10 μM of the three ssDNAs, 20 mM Tris-HCl buffer (pH 8.0), 350 mM NaCl, 1× SYBR® Gold was prepared. Capsular DNA coacervates form inside the W/O microdroplets, as described above. After annealing the DNA solution inside the W/O microdroplets, it precipitated at the bottom of the PCR tube. The lipid-containing oil was then removed from the supernatant. Subsequently, 40 μL of fresh lipid-free oil was added to the PCR tube and pipetted. After 1 h, the W/O microdroplets precipitated at

the bottom of the PCR tube. The oil-exchange process from lipid-containing to lipid-free oil was repeated. After 1 h, the oil in the supernatant was removed entirely. Then, 20 μL of the buffer containing 20 mM Tris-HCl buffer (pH 8.0) and 350 mM NaCl was added into the PCR tube. A hole was made at the bottom of the PCR tube with a pushpin, and the DNA microcapsules were collected through the hole and poured into another PCR tube.

Manipulation of the round porous DNA microcapsules

An observation chamber was constructed (the detailed methods are shown in Figure S3). A round porous DNA microcapsule solution (20 μL) was placed in the chamber, and 20 μL of PEG solution (2.5 wt%, Mw=300,000–500,000) was added to the chamber using a pipette. Morphological changes in the round porous DNA microcapsules were observed using confocal laser scanning microscopy with a UPLSAPO 40× objective lens.

ASSOCIATED CONTENT

Supporting Information.

The following files are available free of charge.

AUTHOR INFORMATION

Corresponding Authors

* Masahiro Takinoue − takinoue@c.titech.ac.jp

* Miho Yanagisawa − myanagisawa@g.ecc.u-tokyo.ac.jp

Present Addresses

M.M. Biomedical Research Institute, National Institute of Advanced Industrial Science and Technology (AIST), 1-1-1 Higashi, Tsukuba, Ibaraki 305-8566, Japan.

Author Contributions

M.T. and M.Y. designed the study. M.M., and M.T. performed the experiments. T.S. performed numerical simulations. M.T. and T.S. performed mathematical analyses. M.T., M.M., and M.Y. wrote the manuscript. All authors discussed the data and revised the manuscript accordingly.

ACKNOWLEDGMENT

We thank Prof. M. Ichikawa (Kyoto University), Prof. T. Hamada (JAIST), Prof. K. Yoshikawa (Doshisha University and Kyoto University), Ms. R. Watanabe (Tokyo Technology), and Prof. Y. Sato (Kyushu Institute of Technology) for fruitful discussions. This work was supported by Human Frontier Science Program (HFSP; RGP0016/2022-102) and the MEXT/JSPS KAKENHI, Japan: a Grant-in-Aid for Transformative Research Areas “Genome Modality” (No. 20H05935), and Grant-in-Aid for Scientific Research S (No. 20H05701) to S.M.N. and M.T.; a Grant-in-Aid for Scientific Research A (No. 20H00619) to M.T.; a Grant-in-Aid for Scientific Research on Innovative Area “Molecular Robotics” (No. 24104002 and No. 25104522) to M.T., M.Y., S.M.N. and S.M; a Leading Initiative for Excellent Young Researchers (16812285), Young Scientists B (No. 16K21034), and a Research Fellowship for Young Scientists (14J10002) to M.M. This work was also supported by the Research Grant Program of the Asahi Glass Foundation and the Support for Tokyo Tech Advanced Researchers (STAR) awarded to M.T.

REFERENCES

(1) Luisi, P. L. The Emergence of Life: From Chemical Origins to Synthetic Biology, Cambridge University Press: **2006**

(2) Jia, T.Z.; Hentrich, C.; Szostak, J.W. Rapid RNA Exchange in Aqueous Two-Phase System and Coacervate Droplets. *Orig. Life Evol. Biosph.* **2014**, *44*, 1–12.

(3) van Swaay, D.; Tang, T.-Y. D.; Mann, S.; de Mello, A. Microfluidic Formation of Membrane-Free Aqueous Coacervate Droplets in Water. *Angew. Chem. Int. Ed.* **2015**, *54*, 8398–8401.

(4) Qiao, Y.; Li, M.; Booth, R.; Mann, S. Predatory Behaviour in Synthetic Protocell Communities. *Nat. Chem.* **2017**, *9*, 110–119.

(5) Douliez, J.-P.; Martin, N.; Gaillard, C.; Beneyton, T.; Baret, J.- C.; Mann, S.; Beven, L. Catanionic Coacervate Droplets as a Surfactant-Based Membrane-Free Protocell Model. *Angew. Chem., Int. Ed.* **2017**, *56*, 13689−13693.

(6) Deng, N. N.; Huck, W. T. S. Microfluidic Formation of Monodisperse Coacervate Organelles in Liposomes. *Angew. Chem., Int. Ed.* **2017**, *56*, 9736−9740.

(7) Samanta, A.; Sabatino, V.; Ward, T. R. Walther, A. Functional and Morphological Adaptation in DNA Protocells via Signal Processing Prompted by Artificial Metalloenzymes. *Nat. Nanotechnol.* **2020**, *15*, 914–921.

(8) Liu, W.; Lupfer, C.; Samanta, A.; Sarkar, A.; Walther, A. Switchable Hydrophobic Pockets in DNA Protocells Enhance Chemical Conversion. *J. Am. Chem. Soc.* **2023**, *145*, 7090–7094.

(9) Crowe, C. D.; Keating, C. D. Liquid-Liquid Phase Separation in Artificial Cells. *Interface Focus* **2018**, *8*, 20180032.

(10) Deshpande, S.; Brandenburg, F.; Lau, A.; Last, M. G. F.; Spoelstra, W. K.; Reese, L.; Wunnava, S.; Dogterom, M.; Dekker, C. Spatiotemporal Control of Coacervate Formation within Liposomes. *Nat. Commun.* **2019**, *10*, 1800.

(11) Mu, W.; Ji, Z.; Zhou, M.; Wu, J.; Lin, Y.; Qiao, Y. Membrane-Confined Liquid-Liquid Phase Separation Toward Artificial Organelles. *Sci. Adv.* **2021**, *7*, eabf9000.

(12) Dolgin. E. Cell Biology's New Phase. *Nature* **2018**, *555*, 300–302.

(13) Brangwynne, C. P.; Tompa, P.; Pappu, R. Polymer Physics of Intracellular Phase Transitions. *Nat. Phys.* **2015**, *11*, 899–904.

(14) Alberti, S.; Gladfelter, A.; Mittag, T. Considerations and Challenges in Studying Liquid-Liquid Phase Separation and Biomolecular Condensates. *Cell* **2019**, *176*(3), 419–434.

(15) Ryden, J.; Albertsson, P.-Å. Interfacial Tension of Dextran-Polyethylene Glycol-Water Two-Phase Systems. *J. Colloid Interface Sci.* **1971**, *37*, 219–222.

(16) Long, M. S.; Jones, C. D.; Helfrich, M. R.; Mangeney-Slavin, L. K.; Keating, C. D. Dynamic Microcompartmentation in Synthetic Cells. *Proc. Natl. Acad. Sci. U. S. A.* **2005**, *102*(17), 5920–5925.

(17) Tsumoto, K.; Arai, M.; Nakatani, N.; Watanabe, S. N.; Yoshikawa, K. Does DNA Exert an Active Role in Generating Cell-Sized Spheres in an Aqueous Solution with a Crowding Binary Polymer? *Life* **2015**, *5*(1), 459–466.

(18) Nakatani, N.; Sakuta, H.; Hayashi, M.; Tanaka, S.; Takiguchi, K.; Tsumoto, K.; Yoshikawa, K. Specific Spatial Localization of Actin and DNA in a Water/Water Microdroplet: Self-Emergence of a Cell- Like Structure. *ChemBioChem* **2018**, *19*(13), 1370–1374.

(19) Sakuta, H.; Fujita, F.; Hamada, T.; Hayashi, M.; Takiguchi, K.; Tsumoto, K.; Yoshikawa, K. Self-Emergent Protocells Generated in an Aqueous Solution with Binary Macromolecules through Liquid-Liquid Phase Separation. *ChemBioChem* **2020**, *21*(23), 3323–3328.

(20) Rowland, A. T.; Keating C. D. Formation and Properties of Liposome-Stabilized All-Aqueous Emulsions Based on PEG/Dextran, PEG/Ficoll, and PEG/Sulfate Aqueous Biphasic Systems. *Soft Matter* **2021**, *17*, 3688–3699.

(21) Masukawa, M. K.; Okuda, Y.; Takinoue, M. Aqueous Triple-Phase System in Microwell Array for Generating Uniform-Sized DNA Hydrogel Particles. *Front. Genet.* **2021**, *12*, 705022.

(22) Shin, Y.; Brangwynne, C. P. Liquid Phase Condensation in Cell Physiology and Disease. *Science* **2017**, *357*, eaaf4382.

(23) Biffi, S.; Cerbino, R.; Bomboi, F.; Paraboschi, E. M.; Asselta, R.; Sciortino, F.; Bellini, T. Phase Behavior and Critical Activated Dynamics of Limited-Valence DNA Nanostars. *Proc. Natl. Acad. Sci. U. S. A.* **2013**, *110*(39), 15633–15637.

(24) Nguyen, D. T.; Saleh, O. A. Tuning Phase and Aging of DNA Hydrogels through Molecular Design. *Soft Matter* **2017**, *13*, 5421–5427.

(25) Jeon, B.-J.; Nguyen, D. T.; Abraham, G. R.; Conrad, N.; Fygenson, D. K.; Saleh, O. A. Salt-Dependent Properties of a Coacervate-Like, Self-Assembled DNA Liquid. *Soft Matter* **2018**, *14*, 7009–7015.

(26) Nguyen, D. T.; Jeon, B.-J.; Abraham, G. R.; Saleh, O. A. Length-Dependence and Spatial Structure of DNA Partitioning into a DNA Liquid. *Langmuir* **2019**, *35*(46), 14849–14854.

(27) Fraccia, T. P.; Jia T. Z. Liquid Crystal Coacervates Composed of Short Double-Stranded DNA and Cationic Peptides. *ACS Nano* **2020**, *14*(11), 15071–15082.

(28) Martin, N.; Tian, L.; Spencer, D.; Coutable-Pennarun, A.; Anderson J. L. R.; Mann, S. Photoswitchable Phase Separation and Oligonucleotide Trafficking in DNA Coacervate Microdroplets. *Angew. Chem., Int. Ed.* **2019**, *58*, 14594−14598.

(29) Wee, W. A.; Sugiyama, H.; Park, S. Photoswitchable Single-Stranded DNA-Peptide Coacervate Formation as a Dynamic System for Reaction Control. *iScience* **2021**, *24*, 103455.

(30) Tanaka, H. Formation of Network and Cellular Structures by Viscoelastic Phase Separation. *Adv. Mater.* **2009**, *21*(18), 1872−1880.

(31) Tanaka, H. Universality of Viscoelastic Phase Separation in Dynamically Asymmetric Fluid Mixtures. *Phys. Rev. Lett.* **1996**, *76*(5), 787.

(32) Araki, T.; Tanaka, H. Simple Tools for Complex Phenomena: Viscoelastic Phase Separation Captured by Disconnectable Springs. *Phys. Rev. E* **2005**, *72*, 041509.

(33) Tanaka, H. Viscoelastic Phase Separation in Biological Cells. *Commun. Phys.* **2022**, *5*, 167.

(34) Iborra, F. J. Can Visco-Elastic Phase Separation, Macromolecular Crowding and Colloidal Physics Explain Nuclear Organisation? *Theor. Biol. Med. Model.* **2007**, *4*, 15.

(35) Seeman, N.; Sleiman, H. DNA Nanotechnology. *Nat. Rev. Mater.* **2018**, *3*, 17068.

(36) Sato, Y.; Sakamoto, T.; Takinoue, M. Sequence-Based Engineering of Dynamic Functions of Micrometer-Sized DNA Droplets. *Sci. Adv.* **2020**, *6*, eaba3471.

(37) Jeon, B.-J.; Nguyen, D. T.; Saleh, O. A. Sequence-Controlled Adhesion and Microemulsification in a Two-Phase System of DNA Liquid Droplets. *J. Phys. Chem. B.* **2020**, *124*(40), 8888–8895.

(38) Saleh, O. A.; Jeon, B.-J.; Liedl, T. Enzymatic Degradation of Liquid Droplets of DNA is Modulated near the Phase Boundary. *Proc. Natl. Acad. Sci. U. S. A.* **2020**, *117*(28), 16160–16166.

(39) Walczak, M.; Brady, R. A.; Mancini, L.; Contini, C.; Rubio-Sánchez, R.; Kaufhold, W. T.; Cicuta, P.; Di Michele, L. Responsive Core-Shell DNA Particles Trigger Lipid-Membrane Disruption and Bacteria Entrapment. *Nat. Commun.* **2021**, *12*, 4743.

(40) Gong, J.; Tsumura, N.; Sato, Y.; Takinoue, M.; Computational DNA Droplets Recognizing miRNA Sequence Inputs Based on Liquid–Liquid Phase Separation. *Adv. Funct. Mater*. **2022**, *32* 2202322.

(41) Leathers, A.; Walczak, M.; Brady, R. A.; Al Samad, A.; Kotar, J.; Booth, M. J.; Cicuta, P.; Di Michele, L. Reaction-Diffusion Patterning of DNA-Based Artificial Cells. *J. Am. Chem. Soc.* **2022**, *144*(38), 17468–17476.

(42) Deng, J.; Walther, A. Programmable ATP-Fueled DNA Coacervates by Transient Liquid-Liquid Phase Separation. *Chem* **2020**, *6*, 3329–3343.

(43) Lee, T.; Do, S.; Lee, J. G.; Kim, D-N.; Shin, Y. The Flexibility-Based Modulation of DNA Nanostar Phase Separation. *Nanoscale* **2021**, *13*, 17638–17647.

(44) Agarwal, S.; Osmanovic, D.; Klocke, M. A.; Franco, E. The Growth Rate of DNA Condensate Droplets Increases with the Size of Participating Subunits. *ACS Nano* **2022**, *16*(8), 11842–11851.

(45) Saleh, O. A.; Wilken, S.; Squires, T. M.; Liedl, T. Vacuole Dynamics and Popping-Based Motility in Liquid Droplets of DNA. *Nat. Commun.* **2023**, *14*, 3574.

(46) Sato, Y.; Takinoue, M. Sequence-Dependent Fusion Dynamics and Physical Properties of DNA Droplets. *Nanoscale Adv.* **2023**, *5*, 1919−1925.

(47) Udono, H.; Gong, J.; Sato, Y.; Takinoue, M. DNA Droplets: Intelligent, Dynamic Fluid. *Adv. Biology* **2023**, *7*, 2200180.

(48) Takinoue, M., DNA droplets for intelligent and dynamical artificial cells: from the viewpoint of computation and non-equilibrium systems. *Interface Focus* **2023**, *13*, 20230021.

(49) Zadeh, J. N.; Steenberg, C. D.; Bois, J. S.; Wolfe, B. R.; Pierce, M. B.; Khan, A. R.; Dirks, R. M.; Pierce, N. A. NUPACK: Analysis and Design of Nucleic Acid Systems, *J. Comput. Chem.* **2011**, *32*, 170−173.

(50) Douglas, S. M.; Marblestone, A. H.; Teerapittayanon, S.; Vazquez, A.; Church, G. M.; Shih, W. M. Rapid Prototyping of 3D DNA-Origami Shapes with caDNAno, *Nucleic Acids Res.* **2009**, *37*(15), 5001–5006.

(51) Doye, J. P. K.; Ouldridge, T. E.; Louis, A. A.; Romano, F.; Šulc, P.; Matek, C.; Snodin, B. E. K.; Rovigatti, L.; Schreck, J. S.; Harrison, R. M.; Smith, W. P. J. Coarse-Graining

DNA for Simulations of DNA Nanotechnology. *Phys. Chem. Chem. Phys.* **2013**, *15*(47), 20395–20414.

(52) Zhang, F.; Nangreave, J.; Liu, Y.; Yan, H. Structural DNA Nanotechnology: State of the Art and Future Perspective. *J. Am. Chem. Soc.* **2014**, *136*(32), 11198–11211.

(53) Um, S.; Lee, J.; Park, N.; Kwon, S. Y.; Umbach, C. C.; Luo, D. Enzyme-Catalysed Assembly of DNA Hydrogel. *Nat. Mater.* **2006**, *5*, 797–801.

(54) Cheng, W.; Campolongo, M.; Cha, J.; Tan S. J.; Umbach, C. C.; Muller, D. A.; Luo, D. Free-Standing Nanoparticle Superlattice Sheets Controlled by DNA. *Nat. Mater.* **2009**, *8*, 519–525.

(55) Lee, J. B.; Peng, S.; Yang, D.; Roh, Y. H.; Funabashi, H.; Park, N.; Rice, E. J.; Chen, L.; Long, R.; Wu, M.; Luo, D. A Mechanical Metamaterial Made from a DNA Hydrogel. *Nat. Nanotechnol.* **2012**, *7*, 816–820.

(56) Kasahara, Y.; Sato, Y.; Masukawa, M. K.; Okuda, Y.; Takinoue, M. Photolithographic Shape Control of DNA Hydrogels by Photo-Activated Self-Assembly of DNA Nanostructures. *APL Bioeng.* **2020**, *4*(1), 016109.

(57) Langecker, M.; Arnaut, V.; Martin, T. G.; List, J.; Renner, S.; Mayer, M.; Dietz, H.; Simmel, F. C. Synthetic Lipid Membrane Channels Formed by Designed DNA Nanostructures. *Science* **2012**, *338*(6109), 932–936.

(58) Czogalla, A.; Kauert, D. J.; Franquelim, H. G.; Uzunova, V.; Zhang, Y. X.; Seidel, R.; Schwille, P. Amphipathic DNA Origami Nanoparticles to Scaffold and Deform Lipid Membrane Vesicles. *Angew. Chem., Int. Ed.* **2015**, *54*, 6501−6505.

(59) Suzuki, Y.; Endo, M.; Sugiyama, H. Lipid-Bilayer-Assisted Two-Dimensional Self-Assembly of DNA Origami Nanostructures. *Nat. Commun.* **2015**, *6*, 8052.

(60) Ishikawa, D.; Suzuki, Y.; Kurokawa, C.; Ohara, M.; Tsuchiya, M.; Morita, M.; Yanagisawa, M.; Endo, M.; Kawano, R.; Takinoue, M. DNA Origami Nanoplate-Based Emulsion with Designed Nanopore Function. *Angew. Chem., Int. Ed.* **2019**, *58*(43), 15299−15303.

(61) Kurokawa, C.; Fujiwara, K.; Morita, M.; Kawamata, I.; Kawagishi, Y.; Sakai, A.; Murayama, Y.; Nomura, S. I. M.; Murata, S.; Takinoue, M.; Yanagisawa, M. DNA Cytoskeleton for Stabilizing Artificial Cells. *Proc. Natl. Acad. Sci. U. S. A.* **2017**, *114*, 7228–7233.

(62) Merindol, R.; Loescher, S.; Samanta, A.; Walter, A. Pathway-Controlled Formation of Mesostructured All-DNA Colloids and Superstructures. *Nat. Nanotechnol.* **2018**, *13*, 730–738.

(63) Samanta, A.; Sabatino, V.; Ward, T. R.; Walter, A. Functional and Morphological Adaptation in DNA Protocells via Signal Processing Prompted by Artificial Metalloenzymes. *Nat. Nanotechnol.* **2020**, *15*, 914–921.

(64) Hamada, S.; Yancey, K. G.; Pardo, Y.; Gan, M.; Vanatta, M.; An, D.; Hu, Y.; Derrien, T. L.; Ruiz, R.; Liu, P.; Sabin, J.; Luo, D. Dynamic DNA Material with Emergent Locomotion Behavior Powered by Artificial Metabolism. *Sci. Robot.* **2019**, *4*, eaaw3512.

(65) Sato, Y.; Takinoue, M. Capsule-like DNA Hydrogels with Patterns Formed by Lateral Phase Separation of DNA Nanostructures. *JACS Au* **2022**, *2*(1), 159–168.

(66) Tran, M. P.; Chatterjee, R.; Dreher, Y.; Fichtler, J.; Jahnke, K.; Hilbert, L.; Zaburdaev, V.; Gopfrich, K. A DNA Segregation Module for Synthetic Cells. *Small* **2023**, *19*, 2202711.

(67) Yanagisawa, M.; Nigorikawa, S.; Sakaue, T.; Fujiwara, K.; Tokita, M. Multiple Patterns of Polymer Gels in Microspheres due to the Interplay Among Phase Separation, Wetting, and Gelation. *Proc. Natl. Acad. Sci. U. S. A.* **2014**, *111*, 15894–15899.

(68) Watanabe, C.; Furuki, T.; Kanakubo, Y.; Kanie, F.; Koyanagi, K.; Takeshita, J.; Yanagisawa, M. Cell-Sized Confinement Initiates Phase Separation of Polymer Blends and Promotes Fractionation upon Competitive Membrane Wetting. *ACS Materials Lett.* **2022**, *4*, 1742–1748.

(69) Huizenga, D. E.; Szostak, J. W. A DNA Aptamer that Binds Adenosine and ATP. *Biochemistry* **1995**, *34*, 656–665.

(70) Simmel, F. C.; Yurke, B. Using DNA to Construct and Power a Nanoactuator. *Phys. Rev. E* **2001**, *63*, 041913.

(71) Takinoue, M.; Kiga, D.; Shohda, K.; Suyama, A. Experiments and Simulation Models of a Basic Computation Element of an Autonomous Molecular Computing System. *Phys. Rev. E* **2008**, *78*, 041921.

(72) Takinoue, M.; Suyama, A. Hairpin-DNA Memory Using Molecular Addressing. S*mall* **2006**, *2*, 1244–1247.

(73) Hagiya, M.; Konagaya, A.; Kobayashi, S.; Saito, H.; Murata, S. Molecular Robots with Sensors and Intelligence. *Acc. Chem. Res.* **2014**, *47*, 1681–1690.

FIGURES

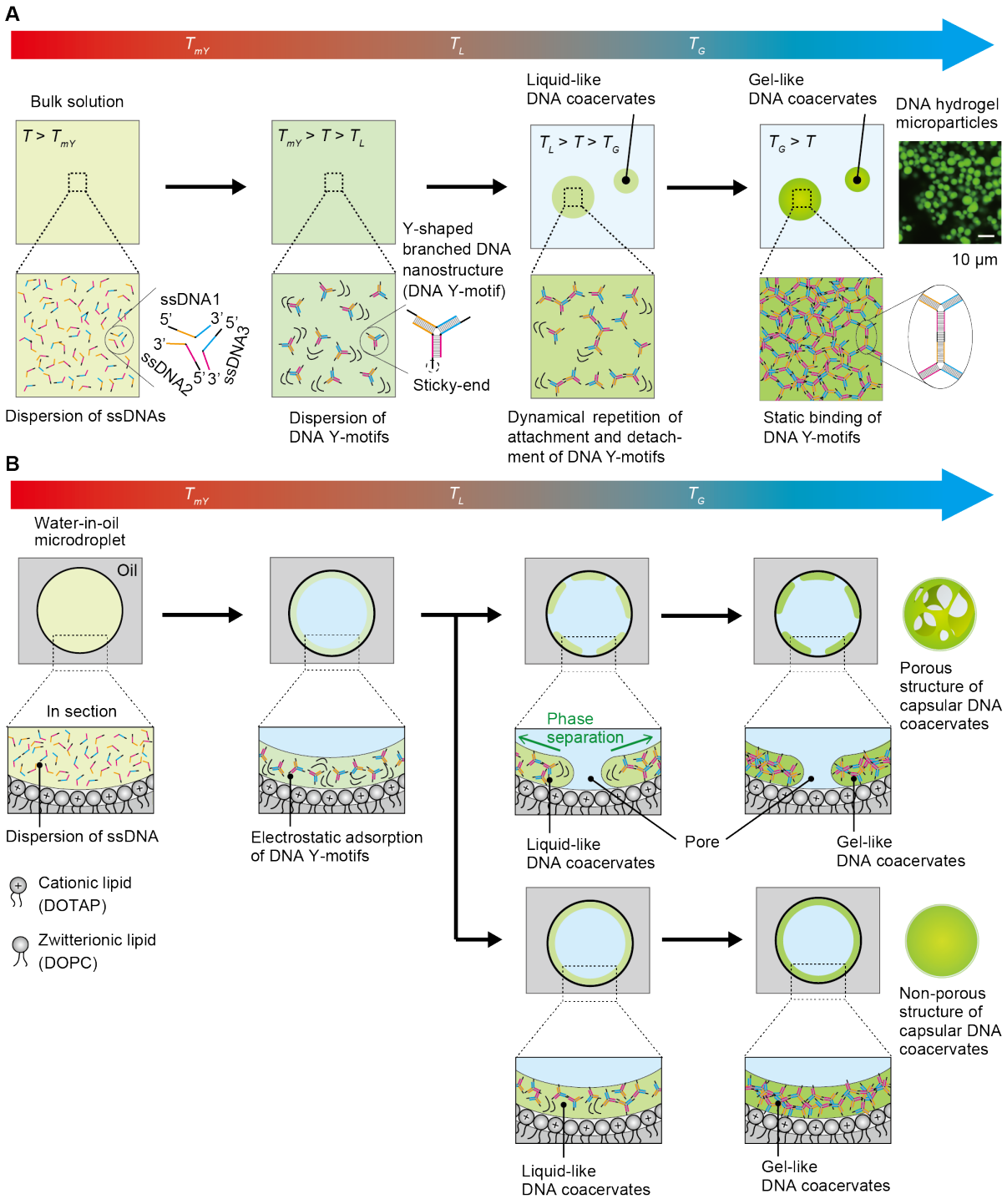

Figure 1. The formation of porous/non-porous structures of capsular DNA coacervates on the interface of W/O microdroplets. (A) Schematic illustration of the formation of liquid- and gel-like DNA coacervates. When the solution temperature $T > T_{mY}$, three kinds of ssDNAs (ssDNA1, ssDNA2, and ssDNA3) are dispersed in the bulk solutions; when $T_{mY} > T > T_L$,

the three ssDNAs form a DNA Y-motif with self-complementary sticky ends; when $T_L > T > T_G$, liquid-like coacervates are formed by the dynamical repetition of attachment and detachment of sticky ends of DNA Y-motifs; when $T_G > T$, gel-like DNA coacervates are formed by the static binding of the DNA Y-motifs via their sticky ends. T_{mY} is the melting temperature of the Y-motif stem. T_L is the formation temperature of liquid-like DNA coacervates. T_G is the formation temperature of gel-like DNA coacervates. (B) Schematic illustration of the formation of porous/non-porous structures of capsular DNA coacervate on the interface of a W/O microdroplet. The W/O microdroplet is covered with a lipid monolayer interface composed of a zwitterionic lipid (DOPC) and a cationic lipid (DOTAP), and the aqueous phase of the W/O microdroplet contains three ssDNAs. By the annealing of the emulsion of W/O microdroplets, the DNA coacervates formed with self-assembly of DNA Y-motifs on the lipid monolayer interface via an electrostatic interaction between the anionic DNA molecules and the cationic interfacial lipids, resulting in the formation of porous/non-porous structures of capsular DNA coacervates.

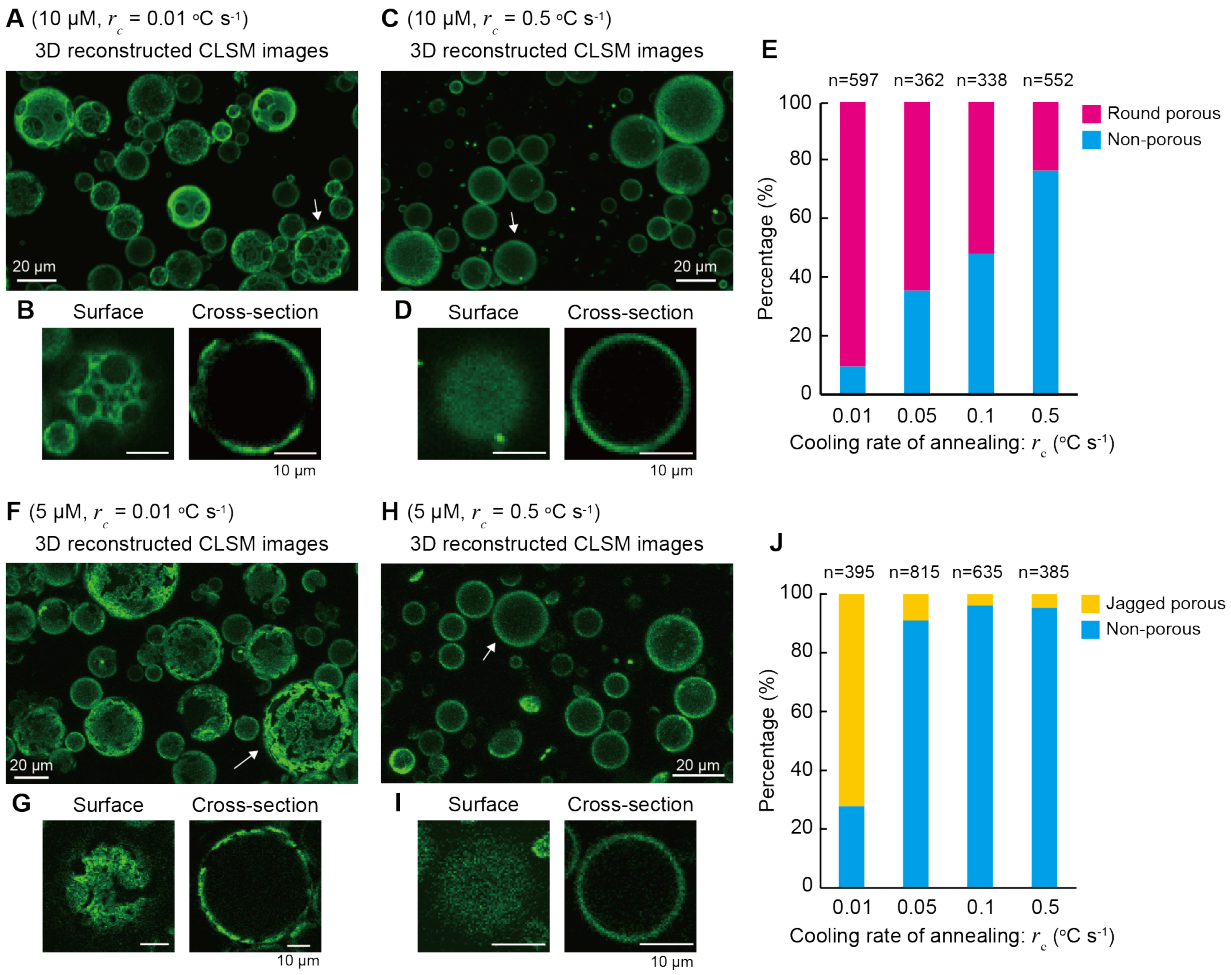

Figure 2. Formation of capsular DNA coacervates on the W/O microdroplet interface. (A) 3D reconstructed CLSM image of round porous structures of capsular DNA coacervates (C_{DNA}= 10 μM; r_c= 0.01°C s^{-1}). (B) CLSM image of the surface and section of the round porous structures of capsular DNA coacervates indicated by the white arrow in (A). (C) 3D reconstructed CLSM image of non-porous structures of capsular DNA coacervates (C_{DNA}= 10 μM; r_c= 0.5°C s^{-1}). (D) CLSM image of the surface and section of the non-porous structures of capsular DNA coacervates indicated by the white arrow in (C). (E) 100% stacked bar chart of porous/non-porous structures of DNA coacervates depending on the cooling rate r_c. (F) 3D reconstructed CLSM image of jagged porous structures of capsular DNA coacervates (C_{DNA}= 5 μM; r_c= 0.01°C s^{-1}). (G) CLSM image of the surface and section of the jagged porous structures of capsular DNA coacervates indicated by the white arrow in (F). (H) 3D

reconstructed CLSM image of non-porous structures of capsular DNA coacervates (C_{DNA}= 5 μM; r_c= 0.5°C s^{-1}). (I) CLSM image of the surface and section of the non-porous structures of capsular DNA coacervates indicated by the white arrow in (H). (J) 100% stacked bar chart of porous/non-porous structures of DNA coacervates depending on the cooling rate r_c. n: number of capsular DNA coacervates in (E) and (J).

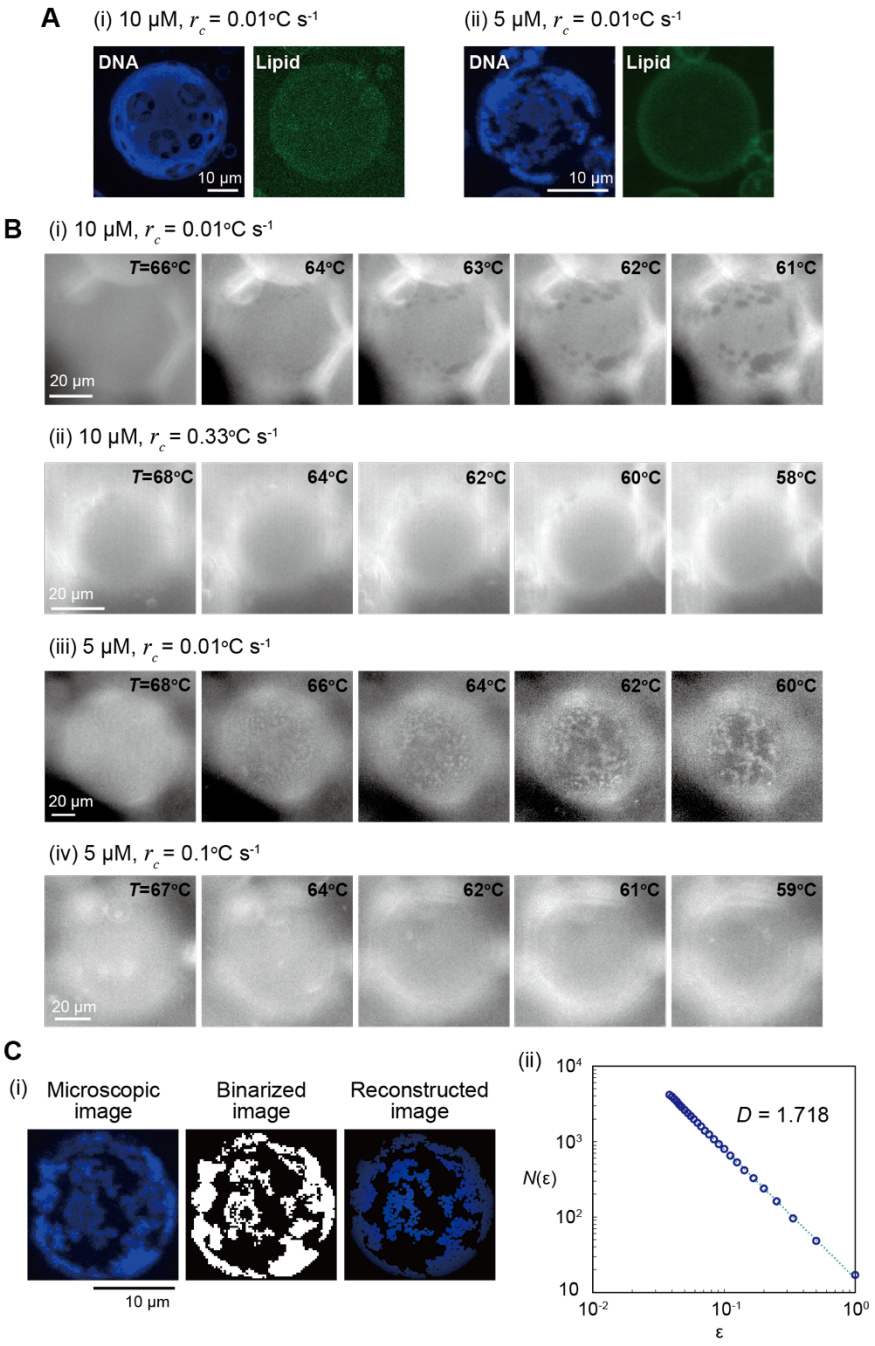

Figure 3. Investigations of the mechanism of porous/non-porous structure formation of capsular DNA coacervates on the W/O microdroplet interface. (A) Comparison between the position of porous structures of capsular DNA coacervates and the distribution of interfacial lipids in various DNA concentrations (i: C_{DNA}= 10 μM, ii: C_{DNA}= 5 μM). DNA: stained with DAPI (blue); DOTAP: stained with NBD-DOTAP (green) (DOPC:DOTAP:NBD-DOTAP = 50:49.9:0.1). (B) Real-time observations of the formation process of porous/non-porous

structures of capsular DNA coacervates on the interface of W/O microdroplets: (i) round porous structures of capsular DNA coacervates (C_{DNA}=10 μM; r_c= 0.01°C s^{-1}) (see also Supplemental Movie 1); (ii) non-porous structures of capsular DNA coacervates (C_{DNA}= 10 μM; r_c= 0.33°C s^{-1}) (see also Supplemental Movie 2); (iii) jagged porous structures of capsular DNA coacervates (C_{DNA}= 5 μM; r_c= 0.01°C s^{-1}) (see also Supplemental Movie 3); (iv) non-porous structures of capsular DNA coacervates (C_{DNA}= 5 μM; r_c= 0.1°C s^{-1}) (see also Supplemental Movie 4). (C) Fractal dimension analysis of the jagged porous structures of capsular DNA coacervates. (i) The reconstruction image (right) obtained from the microscopic image (left) via the binarized image (middle), where the white and black regions correspond to the DNA hydrogel parts and the background, respectively. (ii) Estimation of fractal dimension of microscopic images by the box-counting method: log-log plot of box number $N(\varepsilon)$ as a function of box size ε.

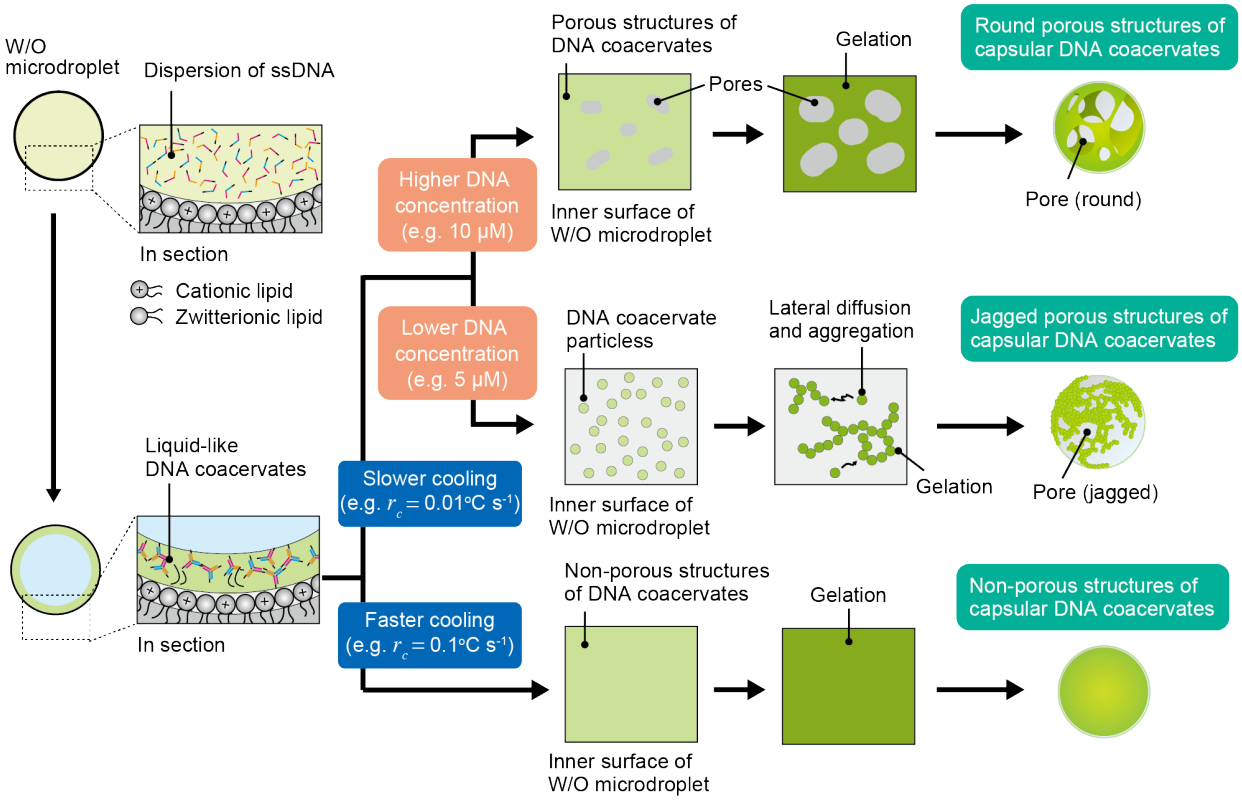

Figure 4. Proposed formation mechanism of porous/non-porous structures of capsular DNA coacervates on the interface of W/O microdroplets.

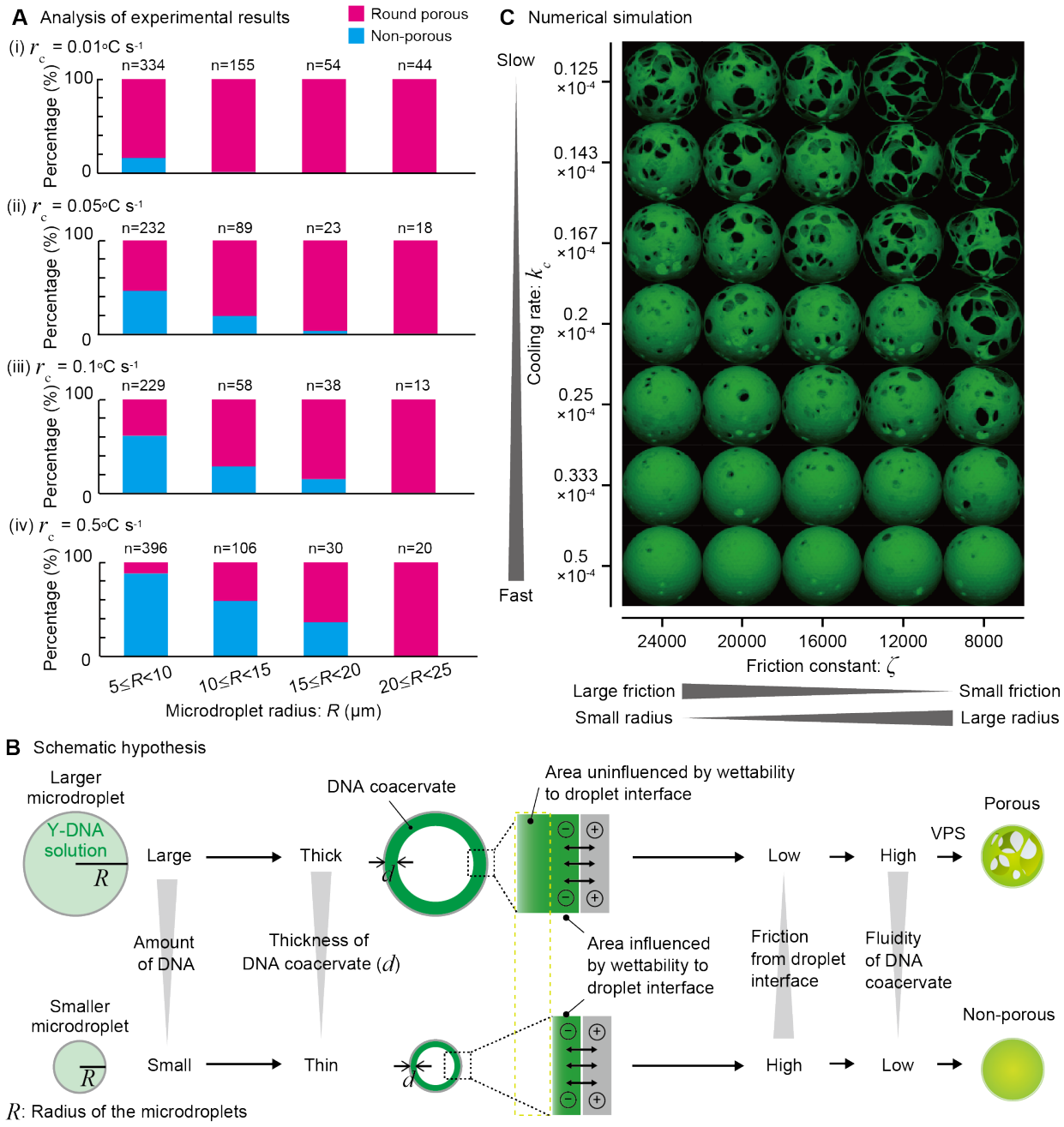

Figure 5. Comparison between numerical simulation results and experimental results about the formation of round porous structures of capsular DNA coacervates. (A) 100% stacked bar chart of porous/non-porous structures of capsular DNA coacervates depending on the W/O microdroplets size in each cooling rate, r_c= 0.01°C s^{-1} (i), r_c= 0.05°C s^{-1} (ii), r_c= 0.1°C s^{-1} (iii) and r_c= 0.5°C s^{-1} (iv). The microdroplets with a radius R < 5 μm were not measured because it was difficult to evaluate small particles accurately. n: number of capsular DNA coacervates.

(B) Hypothesis of the formation of round porous structures of capsular DNA coacervates in the larger W/O microdroplets. (C) Diagram of the numerically simulated structures of DNA coacervate.

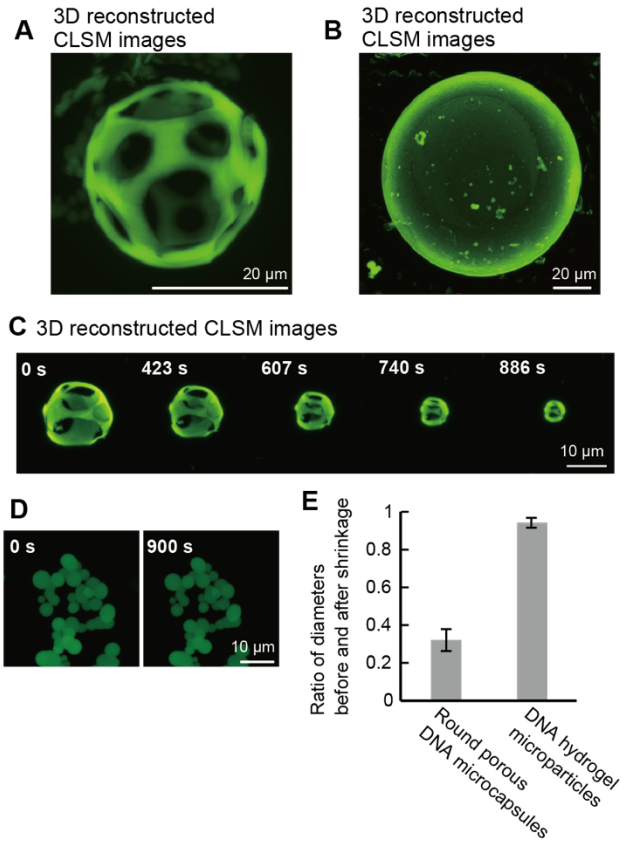

Figure 6. Extraction of gelated capsular DNA coacervates into an aqueous buffer solution from W/O microdroplets and the investigation of the chemical–mechanical responsivity of their structure. (A) 3D reconstructed CLSM image of round porous DNA microcapsule in an aqueous solution (c_{DNA}= 10 µM; r_c= 0.01°C s^{-1}). (B) 3D reconstructed CLSM image of non-porous DNA microcapsule in an aqueous solution (c_{DNA}= 10 µM; r_c= 0.1°C s^{-1}). (C, D) Investigation of the chemical–mechanical responsivity of round porous DNA microcapsules (C) and DNA hydrogel microparticles (D). (C) Shrinkage of the round porous DNA microcapsule after the addition of 1.25% PEG solution (production condition of the microcapsule: c_{DNA}= 10 µM; r_c= 0.01°C s^{-1}). (D) DNA hydrogel microparticles unaltered by the addition of 1.25% PEG solution. (E) Change ratios of diameter before and after the shrinkage of the round porous DNA microcapsules (n=10) and the DNA hydrogel microparticles (n=20).